CI&CEQ
Chemical Industry & Chemical Engineering Quarterly

Available online at
Association of the Chemical Engineers of Serbia AChE
www.ache.org.rs/CICEQ

Chem. Ind. Chem. Eng. Q. 30 (3) 243–256 (2024) CI&CEQ

RADMILA MILENKOVSKA[1]
NIKOLA GESKOVSKI[1]
PETRE MAKRESKI[2]
ANITA GROZDANOV[3]
EMIL POPOVSKI[2]
GJORGJI PETRUSHEVSKI[2,4]
MAJA SIMONOSKA CRCAREVSKA[1]
KRISTINA MLADENOVSKA[1]

[1]Faculty of Pharmacy, Ss. Cyril and Methodius University in Skopje, Skopje, Republic of N Macedonia

[2]Institute of Chemistry, Faculty of Natural Sciences and Mathematics, Ss. Cyril and Methodius University in Skopje, Skopje, Republic of N Macedonia

[3]Faculty of Technology and Metallurgy, Ss. Cyril and Methodius University in Skopje, Skopje, Republic of N Macedonia

[4]Alkaloid AD Skopje, Skopje, Republic of N Macedonia

SCIENTIFIC PAPER

UDC 66.097.3:546.26:54.03

FUNCTIONALIZED CARBON NANOSTRUCTURES AS TEMOZOLOMIDE CARRIERS: PHYSICOCHEMICAL AND BIOPHARMACEUTICAL CHARACTERIZATION

Article Highlights

- Oxidized and noncovalent PEGylated MWCNTs and MWCNTs-G are used as Temozolomide (TMZ) carriers
- Physicochemical characterization confirmed the PEGylation and drug loading in the nanocarriers
- Relatively high encapsulation efficacy and TMZ loading in the carbon nanostructures
- Particle size distribution and zeta potential values suitable for brain tumor delivery
- Sustained TMZ release was observed *in vitro,* indicating controlled drug release in brain tumors

Abstract

In this study, temozolomide (TMZ), a drug used in the treatment of anaplastic astrocytoma and glioblastoma multiforme, was incorporated in multiwalled carbon nanotubes (MWCNTs) and hybrid carbon nanotubes with graphene (MWCNTs-G) functionalized by polyethylene glycol (PEG). The aim was to evaluate the potential of these nanocarriers for targeted delivery and sustained release of TMZ in brain tumor cells. Oxidized MWCNTs and MWCNTs-G were noncovalently functionalized with PEGs of different molecular weights and subsequently loaded with TMZ following standard procedures. Thorough physicochemical and biopharmaceutical characterization of the TMZ-loaded carbon nanocarriers pointed to high encapsulation efficacy (up to 67%) and drug loading (up to 18% out of 25% theoretical value) and homogeneous particle size distribution, with z-average (160 to 300 nm) and zeta potential (-31 to -21 mV) of the particles adequate for crossing the blood-brain-tumor-barrier (BBTB) and entering into the tumor cells. Successful functionalization and TMZ loading were confirmed by SEM and TEM images, UV-Vis absorption, infrared and Raman spectroscopy, and TGA analyses. Sustained release of TMZ from the carbon nanocarriers was observed in vitro. The presented findings form a fundamental platform for further investigation of these formulations against different types of glioma cells and in adequate animal models.

Keywords: multiwalled carbon nanotube, graphene, polyethylene glycol, Temozolomide, physicochemical properties, sustained release.

The limited bioavailability and intrinsic toxicity of many drug substances drive the pharmaceutical industry towards the design and development of novel drug carriers, with a capacity to improve the physicochemical properties of the drugs and overcome the physiological, biochemical, and chemical barriers in their delivery at the site of action. Among them are carbon nanostructures such as graphene, a single layer of carbon below and above the plane, packed tightly into a hexagonal, honeycomb structure, and carbon nanotubes (CNTs) in the form of elongated enfolded graphene sheets such as single-wall (SWCNTs) and multiple layers of graphene sheets,

Correspondence: K. Mladenovska, Faculty of Pharmacy, Ss. Cyril and Methodius University in Skopje, Blv. Mother Theresa No. 45, 1000 Skopje, Republic of N Macedonia.
E-mail: krml@ff.ukim.edu.mk
Paper received: 5 May, 2023
Paper revised: 25 September, 2023
Paper accepted: 23 November, 2023

https://doi.org/10.2298/CICEQ230505027M

namely multiple-wall carbon nanotubes (MWCNTs) [1]. These carbon materials' excellent mechanical, physical, and chemical properties have made them promising blocks for synthesizing graphene-carbon nanotube hybrid structures (MWCNTs-G). The distinct structural properties of these carbon nanostructures, in particular, nanoscale structure and high aspect ratio, are an appropriate addition to their stability, high adsorption capacity, and suitability for functional modification, making them useful carriers for site-specific and controlled drug delivery. The internal cavities of the nanotubes provided high loading capacity for several therapeutic agents, including anticancer drugs [2,3], proteins [4], gene delivery and gene therapy [5–7], and a wide range of bioactive molecules were also covalently or noncovalently immobilized on the external surface of CNTs for specific targeting [8–10]. Furthermore, the tubular shape of CNTs enables them to better penetrate cell membranes through both receptor-mediated or adsorptive-mediated energy-dependent pathways (transcytosis) and passive energy-independent mechanisms (needle-like crossing) without causing cell changes and death, which is a major advantage compared to other nanocarriers [11].

Due to the oxidation of these carbon nanostructures, carboxylic groups become attached in the presence of concentrated acids, contributing to higher hydrophilicity and biocompatibility [12]. Oxidized nanostructures can be further coated to make them more stable and dispersible in various biological solutions, including serum. When coated with (poly)ethylene glycol (PEG), the dispersion gets extraordinary due to the irreversible adsorption of PEG molecules to the sidewalls of carbon structures through π-stacking, van der Waals, and hydrophobic interactions. In addition, PEG functionalization allows surprisingly high degrees of π-stacking of aromatic molecules, including drugs and combinations of molecules. PEGylated carbon nanostructures display relatively lower cytotoxicity and longer blood circulation half-life, which increases the chance of reaching the cancerous or tumorous tissues/cells and also impedes *in vivo* opsonization and reduces uptake by the reticuloendothelial system (RES). In addition, PEG is resilient under oxidizing and reducing conditions and is sufficiently stable against decomposition induced by acids and bases [13].

Having all these in regard, in the presented study (PEGylated), MWCNTs and MWCNT-G have been prepared as carriers of Temozolomide (TMZ), and their suitability for targeted and controlled delivery at the site of action has been evaluated by physicochemical and biopharmaceutical characterization. TMZ is an imidazotetrazine second-generation alkylating agent with a schedule-dependent anti-tumor activity against highly resistant malignancies, including high-grade malignant gliomas such as glioblastoma multiforme (GBM). GBM is among the most aggressive types of brain tumors, with rapid proliferation, diffuse brain invasion, as well as tumor-induced brain edema and neurodegeneration as pathological hallmarks. TMZ, as a prodrug, crosses the blood-brain barrier (BBB) and is converted *via* hydrolysis under physiological conditions in the active cytotoxic form of 5-(3-methyl-triazen-1-yl) imidazole-4-carboxamide (MTIC) that subsequently methylates DNA in the O^6 position of guanine residues. Considering that MTIC does not cross BBB and exhibits low cell availability, it is paramount to prolong the half-life of TMZ under physiological conditions and promote a greater accumulation at the GBM site prior to degradation in the bloodstream. In this way, the drug would be more effective and safer because lower doses could be administered to maintain the therapeutic level [14].

Several research groups investigated this approach in improving the TMZ therapeutic index by loading it in polylactide-based nanoparticles [15–17]. To our knowledge, this is the first paper in which MWCNTs and MWCNT-G hybrid are used as carriers of TMZ. In addition, carbon nanocarriers were noncovalently functionalized by PEGs of different molecular weights to prepare more soluble/dispersible drug delivery systems, with more active sites for TMZ loading, able to protect TMZ from degradation in the peripheral tissues, prolong its blood circulation half-life and provide greater accumulation in the region of GBM. One also expects that the resemblance of CNTs to specific neuronal structures (e.g., ion channels, signaling proteins, and elements of the neuronal cytoskeleton), as well as electrically conductive capacity and strong mechanical properties, may have an additional benefit to the established aim, with regard to enhancing neuronal interaction at the molecular level, improving the management of the physiological activity of neurons and processing of neuronal information [18].

MATERIALS AND METHODS

Materials

As carriers of TMZ, MWCNTs-COOH (purity > 95 wt.%, number of walls > 2, length 10-30 μm, outer diameter 30-50 nm, -COOH content 0.7 wt%, zeta potential -38*mV*, average size 136±20nm) were purchased from Sisco Research Laboratories Pvt, Ltd, India, while the MWCNTs-G hybrid (purity > 99 wt.%, length < 10 μm, inner diameter < 30 nm, outer diameter 30-100 nm, wall thickness 1-2 nm, zeta potential -29 mV, 810± 42 nm average size) from Incubation

Alliance, Inc., Japan. The MWCNTs-COOH and MWCNTs-G (previously activated to MWCNTs-G-COOH) were noncovalently functionalized by polyethylene glycol (PEGOH(C_2H_4O)n H) of different molecular weights (Mw): average Mw 1400–1600 g/mol, Mn/Mw ~ 1.1 (PEG1500), average Mw 3500–4500 g/mol, Mn/Mw ~ 1.1 (PEG4000) and average Mw 5000–7000 g/mol, Mn/Mw ~ 1.1 (PEG6000), all purchased from Merck Schuchardt OHG, Germany. For the functionalization procedure of the carbon nanostructures, 98% H_2SO_4 and 65% HNO_3 were used, both purchased from Carlo Erba Reagents S.A.S., Italy. TMZ was supplied by Sigma-Aldrich (Saint Louis, USA) and Polysorbate® 80 (Sigma-Aldrich, Poole, UK). All chemicals were of analytical grade.

Methods

Functionalization of carbon nanostructures

In the first step, the MWCNTs-G hybrid was oxidized by a modified procedure described by Zhang *et al.* [4], Zhao *et al.* [12], and Huang *et al.* [19] in which 1 g of MWCNTs-G was added to 400 mL of a mixture of 98% H_2SO_4 and 65% HNO_3 (v/v=3:1) initially equipping with ultrasound for 8 h, with subsequent vigorous stirring at 80 °C for another 8 h. The resulting product was separated by centrifugation (3000 rpm, Eppendorf, MiniSpin, Germany), and the sediment was thoroughly and repeatedly washed with deionized water until it reached neutral pH. Afterward, the oxidized MWCNTs-G (MWCNTs-G-COOH) were dried in an air dryer at 50 °C (ST-01/02, Instrumentaria Zagreb, Croatia).

For noncovalent PEGylation, cut and activated MWCNTs-G-COOH and commercially purchased MWCNTs-COOH, each per 20 mg, were dispersed in ultrapure water (200 mL) and pre-sonicated in an ultrasonic bath for 60 min (Ultrasons-H, J. P. Selecta s.a., Spain). Aqueous solutions of PEG1500, PEG4000, and PEG6000 (3 mg/mL, 20 mL) were added drop-wise into the suspensions accordingly while keeping sonication for another 10 min and then magnetically stirring for 24 h at room temperature (250 rpm, VARIO MAG Multipoint, USA). The samples were collected by centrifugation at 12 000 rpm for 15 min (Eppendorf, MiniSpin, Germany), washed five times with deionized water, and dried overnight under vacuum [20].

Temozolomide loading in PEGylated carbon nanostructures

To 10 mL acidified aqueous solution of TMZ (1 mg/mL, pH 2), 30 mg PEGylated carbon nanostructures were added. The dispersion was sonicated for two hours (Ultrawave Limited, Cardiff, UK) and then magnetically stirred for three days (250 rpm) at room temperature (VARIO MAG Multipoint, USA). Afterward, the drug-loaded carbon nanostructures (MCWNTs-PEG-TMZ and MWCNTs-G-PEG-TMZ) were isolated by centrifugation (12000 rpm, 15 min; Eppendorf, MiniSpin, Germany), washed with double-distilled water and left in air dryer (ST-01/02, Instrumentaria Zagreb, Croatia) at 37 °C during 72 h. For comparison, TMZ was also loaded in non-PEGylated carbon nanostructures, MWCNTs-TMZ and MWCNTs-G-TMZ, using the same procedure.

Biopharmaceutical characterization of Temozolomide loaded PEGylated carbon nanostructures

Drug loading efficacy and content

In all formulations, the efficacy of TMZ loading was determined as described in Eq. (1). The concentration of TMZ in the supernatant (nonencapsulated TMZ) was determined by UV-Vis absorption spectroscopy at λ_{max} 328 nm (UV/VIS Perkin Elmer Lambda 16, Arizona, USA).

$$\text{Drug loading efficacy}(\%) = \frac{total\ TMZ\,(mg) - nonencapsulated\ TMZ\,(mg)}{total\ TMZ\,(mg)} \cdot 100\% \quad (1)$$

The content of TMZ in the carbon nanostructures was determined using Eq. (2).

$$TMZ\ content\,(\%) = \frac{encapsulated\ TMZ\,(mg)}{\text{mass of loaded } MWCNT\ formulation\,(mg)} \cdot 100\% \quad (2)$$

All data were averaged from five measurements at least.

Size distribution and surface charge

The hydrodynamic diameter (z-average), polydispersity index (PDI), and zeta potential of blank and TMZ-loaded carbon nanostructures were determined by dynamic light scattering (NanoZS-100, Malvern Instruments Ltd., Worcestershire, UK) in the wet dispersions. The wet dispersions were prepared by dispersing the formulations (5–10 mg) in phosphate buffer saline (PBS) 0.0001M, by Ultra-turrax (T25 basic, IKA Werke, Cardiff, UK) for 1 min (13500 rpm). A small aliquot of the resulting suspension was transferred to the measurement cell. At least six measurements were done for each sample.

Morphology

The morphology of blank and TMZ-loaded carbon nanostructures was visualized by scanning electron microscopy (SEM, FEI Quanta 200, acceleration voltage 30 kV with EDS Oxford Inca Energy 350,

equipped with a secondary electron detector, UK) and Transmission Electron Microscope (TEM–FEI Tecnai G2 Spirit TWIN equipped with LaB6, UK).

In vitro dissolution test

The release of TMZ from TMZ loaded (non)-PEGylated carbon nanostructures was followed *in vitro*, using the dialysis bag diffusion technique (dialysis membrane Mw cut-off 12000, Sigma-Aldrich, USA). Hermetically sealed formulations (~ 30 mg) were suspended in 50 mL PBS pH 7.4. The experimental temperature was kept at 37 ± 0.5 °C, with continuous magnetic stirring at 100 rpm. At selected time intervals up to 216 h, the drug sample was removed from the receptor compartment with the replacement of the same medium. The concentration of released TMZ was quantified by measuring the concentration of formed active hydrolytic product MTIC at pH 7.4 and 37 °C using UV-Vis absorption spectroscopy (λ_{max} 255 nm, UV/VIS Perkin Elmer Lambda 16, Arizona, USA) [15]. All data were averaged from three measurements.

Physicochemical characterization of Temozolomide loaded PEGylated carbon nanostructures

For physicochemical characterization of TMZ loaded (non)-PEGylated nanostructures with respect to interactions and stability during the preparation procedure, the formulations were characterized using infrared (IR), ultraviolet-visible (UV-Vis), and Raman spectroscopy and thermogravimetric analysis (TGA) as well.

Infrared spectroscopy

Infrared measurements were performed on blank and TMZ-loaded (non)-PEGylated carbon nanocarriers (2 mg of homogenized samples) using KBr pellets (200 mg dry potassium bromide per pellet). The characteristic absorption bands were recorded in a 4000–400 cm^{-1} wavenumbers range (Varian-660 FT-IR, Agilent Technologies, USA).

Ultraviolet-visible spectroscopy

UV-Vis absorption spectra of all samples were collected in a quartz cell with a 1.0 cm path length using a UV/Vis Perkin Elmer Lambda 16 (Arizona, USA) spectrophotometer.

Raman spectroscopy

Raman spectra were collected on a LabRam 300 Infinity micro-Raman multichannel spectrometer (Horiba JobinYvon, Japan) using the He:Ne laser at 632.81 nm. An 1800 lines/mm grating monochromator received the backscattered radiation (180° configuration). Raman intensities were collected with a thermo-electrically cooled CCD. An Olympus LMPlanFL ×50 objective (N.A = 0.5) with a long working distance (10.6 mm) was used for magnification. A LaserCheckTM Handheld Power Meter (Coherent Scientific, Australia) was used to measure the laser power on the samples, which was 1.82 mW. The spectral collection time was set to 5 seconds, and the spectrum averaged from 5 scans. For calibration purposes, the Rayleigh line at 0 cm^{-1} and the band of a Si standard centered at 520.5 cm^{-1} were used.

Thermogravimetric analysis

The TGA experiment on the same samples (7-10 mg per sample) was performed with a model Pyris 1 TGA (PerkinElmer, Shelton, CT, USA), under nitrogen atmosphere, at a heating rate of 10 °C/min in a temperature range of 30–800 °C.

RESULTS AND DISCUSSION

Biopharmaceutical characterization of Temozolomide loaded PEGylated carbon nanostructures

Loading efficacy, drug content, surface charge, and particle size distribution

The drug loading efficacy and content in all series (Table 1) ranged from 54% to 67% and 14% to 18% (out of 25% theoretical value), respectively, being highest in the MWCNTs-TMZ. Higher values for TMZ loading efficacy and content were obtained for non-PEGylated MWCTs-TMZ and MWCNTs-G-TMZ formulations relative to the adequate PEGylated formulations ($p < 0.05$). The MWCNTs-(PEG-)TMZ formulations demonstrated better TMZ loading capability relative to the hybrid MWCNTs-G-(PEG-)TMZ formulations ($p < 0.05$), while non-significant differences were observed among the PEGylated formulations, both MWCNTs-PEG-TMZ and MWCNTs-G-PEG-TMZ ($p > 0.05$). These data suggest dominantly physical entrapment of TMZ into the tubes, although wrapping around the tubes cannot be excluded. Taking into consideration the medium in which TMZ loading was performed, there could be a possibility for electrostatic interactions and hydrogen bonding from the proton of the carboxyl group in the MWCNTs-COOH/MWCNTs-G-COOH and hydroxyl group in the MWCNTs-PEG/MWCNTs-G-PEG with nitrogen atoms at positions 1, 2 and 7 and oxygen atoms at position 4 and from the amide group in the structure of TMZ (3-methyl-4-oxoimidazo[5,1-d][1,2,3,5]tetrazine-8-carboxamide). In addition, a competition between PEG and TMZ, regarding the entrapment into and the wrapping around the carbon nanostructures, cannot be excluded, despite the observed non-significant influence of a PEG molecular weight on TMZ loading. The slightly higher values for the drug loading observed in MWCNTs formulations, compared to hybrid MWCNTs-G, can be

explained by the lower content of MWCNTs in MWCNTs-G hybrid in which TMZ is dominantly entrapped, also evident by the SEM images (Fig. 1d, e, f).

Table 1. Loading efficacy and content, particle size distribution, and zeta potential of blank and TMZ-loaded activated and PEGylated carbon nanostructures.

Series	Parameters			
	Loading efficacy (± SD, n=6) %	Content (± SD, n=6) % (theor. 25%)	d_{50}/PDI (nm)	Zeta potential (±SD, n=6) *mV*
MWCNTs (-COOH)	/	/	136/0.460	-38.38 ± 0.85
MWCNTs-PEG1500	/	/	185/0.443	-20.73 ± 1.33
MWCNTs-PEG4000	/	/	188/0.422	-21.51 ± 0.75
MWCNTs-PEG6000	/	/	192/0.437	-22.32 ± 1.31
MWCNTs-TMZ	66.96 ± 0.60	17.94 ± 0.60	163/0.385	-27.45 ± 1.37
MWCNTs-PEG1500-TMZ	56.79 ± 5.36	16.63 ± 0.62	201/0.466	-21.25 ± 0.21
MWCNTs-PEG4000-TMZ	56.44 ± 4.71	16.49 ± 0.41	236/0.429	-22.05 ± 0.64
MWCNTs-PEG6000-TMZ	55.41 ± 2.97	15.96 ± 1.29	248/0.301	-24.70 ± 1.33
MWCNTs-G (-COOH)	/	/	222/0.406	-46.05 ± 1.15
MWCNTs-G-PEG1500	/	/	248/0.481	-24.87 ± 0.58
MWCNTs-G-PEG4000	/	/	260/0.321	-24.09 ± 1.56
MWCNTs-G-PEG6000	/	/	276/0.392	-23.24 ± 0.42
MWCNTs-G-TMZ	58.20 ± 1.60	16.11 ± 0.45	255/0.479	-31.23 ± 2.02
MWCNTs-G-PEG1500-TMZ	58.64 ± 4.83	14.99 ± 1.29	264/0.485	-25.25 ± 0.91
MWCNTs-G-PEG4000-TMZ	56.98 ± 3.07	14.58 ± 0.43	278/0.385	-25.90 ± 0.83
MWCNTs-G-PEG6000-TMZ	54.97 ± 6.13	14.40 ± 1.25	303/0.372	-25.95 ± 0.55

The zeta potential in physiologically relevant pH was determined (Table 1) to examine the surface properties of the carbon nanocarriers. The commercially activated MWCNTs-COOH had a zeta potential of around –38 mV, while the negative zeta potential of approx. –26 mV for MWCNTs-G increased to approx. –46 mV due to COO^- groups on the surface of the functionalized MWCNTs-G-COOH carbon nanocarriers. The PEG functionalization of the carbon nanocarriers led to decreased zeta potential, most likely due to the capping of the surface-oriented -COOH groups. When TMZ was loaded in the non-PEGylated carbon nanocarriers, the zeta potential also decreased, probably due to the electrostatic interactions between the carbon carriers and TMZ and the location of TMZ into/on the carriers. A similar trend was not observed for the PEG functionalized carbon nanocarriers (Table 1), as the neutral PEG chains had already covered the carboxyl groups. Moreover, a non-significant difference in zeta potential between all PEGylated series was observed, thus implying the PEG dominance on the surface properties of the functionalized nanocarriers. Furthermore, loaded PEGylated carbon nanocarriers showed significantly lower negative zeta potential value compared to TMZ-loaded non-PEGylated carriers (Table 1), which confirms the effective PEG capping of the carboxylic end groups from the carbon nanocarriers.

These results correspond with the literature data on TMZ loaded in transferrin-appended PEGylated PLGA nanoparticles [21]. It is well-known that PEG's protective (stealth) action in the PEGylated nanoparticles is mainly due to the formation of a dense, hydrophilic cloud of flexible chains on the surface of the particles that reduces the hydrophobic interaction with the RES. Therefore, tethered and anchored PEG chains on the TMZ-loaded carbon nanostructures could prevent the opsonization of the particles by the RES macrophages, leading to a prolonged circulation time of the particles in the blood and preferential accumulation in the brain tumor cells.

Various literature data exist on the influence of the particle's surface charge on their internalization into the tumor cells. The surfaces of cancer cells are negatively charged due to the translocation of negatively charged constituents from the inner envelope of the cell membrane. However, in the intracellular space, a low pH prevails (around 5.7–7.4), depending on the tumor's histology, volume, and location [22]. Electrostatic interactions mediate the uptake of nanoparticles into the central nervous system (CNS) between positively charged ligands and negatively charged membranes of the BBB cells. Having this in regard, positively charged

particles have an advantage in drug delivery across the BBB. They bind to anionic sites on the luminal surface of brain capillaries (derived from sialic acid residues of glycoproteins) and undergo absorptive-mediated endocytosis [23]. However, the presence of positively charged groups on their surface may increase non-specific uptake and reduce the efficiency of targeted delivery into the CNS due to binding to negatively charged plasma proteins. The advantage of particles with neutral and negative zeta potential is the lower adsorption of proteins on their surface in the circulation, as well as the lower ability to accumulate in the liver and spleen compared to positively charged nanoparticles [24]. Accordingly, during the distribution in the central circulation, the particles should have a negative or neutral zeta potential, while at the point of passage through the BBB, particles with a positive charge have an advantage. The different pH values in the blood circulation and healthy cells compared to tumor cells give the possibility to change the surface charge of the particles at the site of internalization, which was shown in a study with carbon nanotubes loaded with zwitterionic doxorubicin [25]. Hence, for effective delivery of nanoparticles into the tumor cells, a neutral or weakly negative charge upon i.v. application and a change in positive charge upon arrival at the tumor site are desired. Most nanoparticle formulations in the literature for brain delivery have moderately negative (between -1 mV and -15 mV) or high (between 15 mV and 45 mV) negative potential. It is also mentioned that formulations with moderate (up to 15 mV) or high positive zeta potential (above 15 mV) can pass through the BBB and, in some instances, have been proven to be effective delivery systems in the brain. Based on these literature data, the surface charge of the prepared carbon nanoformulations with TMZ suggests the potential for their delivery into the brain, that is, for treating brain tumors [26].

The z-average size of the activated MWCNTs-COOH and MWCNTs-G-COOH increased from around 136 nm and 222 nm to 163 nm and 255 nm, respectively, when TMZ was loaded (Table 1). After the PEG coating, the initial particle size also increased, being the highest in the formulations coated with PEG6000 (around 192 nm and 276 nm, respectively). When TMZ was loaded, an additional non-significant increase was evident, with the z-average between 201 nm (MWCNs-PEG1500-TMZ) and 303 nm (MWCNTs-G-PEG6000-TMZ). In all PEGylated series with TMZ, a relatively unimodal particle size distribution was observed, with PDI values not exceeding 0.485.

The size of the particles significantly affects their *in vivo* behavior and distribution. Larger size nanoparticles have a greater tendency after i.v. application to be trapped by the lungs, while the smaller ones to be eliminated through the kidneys. Also, particles larger than 200 nm tend to activate the lymphatic system and be more quickly removed from the circulation [27]. The particle size also affects the permeability across the BBTB. Compared to blood-tumor barriers, BBTB is characterized by smaller pores, indicating that larger delivery systems will have difficulty entering the brain tumor. For most of the particles intended for brain (tumor) delivery, a median size of 200 nm is commonly reported [28], a statistical value indicating a range from 50 to 400 nm. The size distribution of the TMZ-loaded formulations in the current study did not exceed these limits, pointing to their potential for crossing the BBTB. However, although most studies note greater anti-tumor efficacy of shorter CNTs [29], there are also literature data indicating that the cellular accumulation of CNTs is independent of length/size (studies with length distribution of SWCNTs and MWCNTs between 195 nm and 630 nm) [30]. Our data are very similar to the data obtained in the study of Ren *et al.* [31] in which dual-functionalized MWCNTs subsequently loaded with doxorubicin, with size between 147 and 202 nm (and zeta potential between -8 mV and -29 mV) were able to cross the BB(T)B and accumulate into the brain tumor cells *in vitro* in BCEC and C6 cells and *in vivo* in intracranial C6 glioma bearing Balb/c mice.

Morphology

The surface morphology of the TMZ loaded and unloaded PEGylated MWCNTs and MWCNTs-G hybrid was studied using SEM and TEM imaging (Fig. 1).

The SEM image of MWCNTs-COOH (Fig. 1a) shows a dense structure comprised of randomly aggregated highly tangled tubes. In the SEM and TEM images of MWCNTs-TMZ (Figs. 1b and 1h, respectively), the entrapment of TMZ into the tubes and its presence on the MWCNTs surface can be seen. The functionalization of the MWCNTs with PEG in the MWCNTs-PEG-TMZ was also confirmed by the non-uniform surface, which can be seen from the SEM and TEM images (Figs. 1c and 1i, respectively).

No clear distinction in the morphology between TMZ-loaded and non-loaded MWCNTs-PEG was observed with the imaging techniques. In the images of the MWCNTs-G hybrid (Fig. 1d–f), one can see that the MWCNTs are incorporated into the graphene layers, while the surface morphology exhibits a mixed structure with MWCNTs dispersed between different graphene sheets due to the interactions between the hydrophobic region of graphene and the side walls of MWCNTs. In Fig. 1h and 1i, bulging from the loaded TMZ and surface roughness can be seen due to the functionalization with PEG.

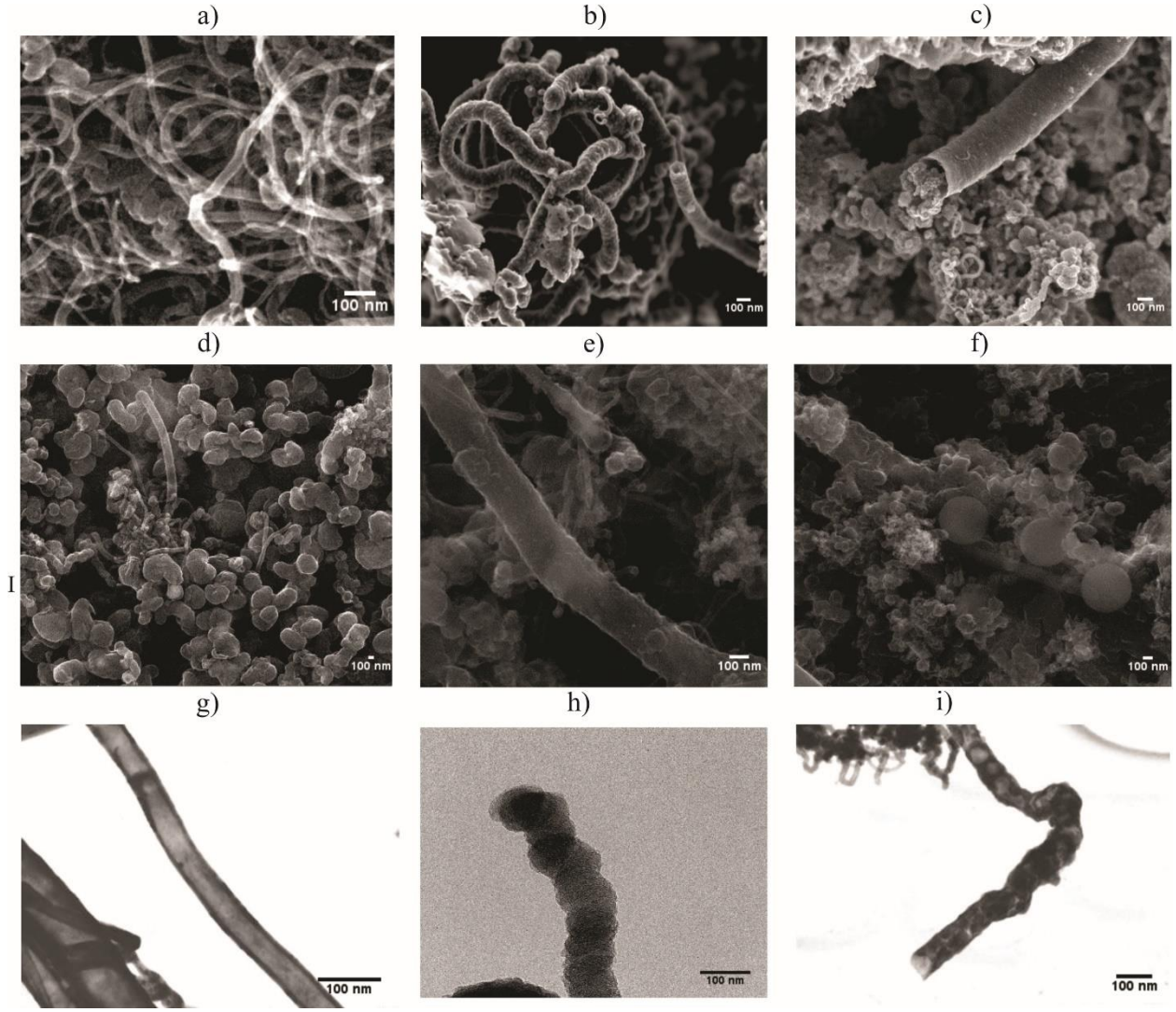

Figure 1. SEM images of (a) MWCNTs-COOH; (b) MWCNTs-TMZ; (c) MWCNTs-PEG-TMZ (x 50.000 mag.); (d) MWCNTs-G-COOH; (e) MWCNTs-G-TMZ; (f) MWCNTs-G-PEG-TMZ; the scale bar presents 100 nm and TEM images showing (g) MWCNTs-COOH; (h) MWCNTs-TMZ; (i) MWCNTs-PEG6000-TMZ.

In vitro drug release

Metabolic remodeling with increased glucose uptake compared to normal brain cells is a characteristic feature of glioblastoma. To sustain tumor cell proliferation and tumor growth, tumor cells increase their glycolytic activity, and additionally, most of the metabolized glucose is converted into lactate. Together with glutaminolysis, these two mechanisms are the major suppliers of lactic and carbonic acid concentrations in tumor cells. However, despite the high acid concentration in brain tumor cells, their intracellular pH is neutral (pH ~7.4) [32], which was the rationale for performing the *in vitro* dissolution studies in a medium with pH 7.4.

Regarding the TMZ release profile, all formulations (except MWCNTs-G-TMZ) showed a biphasic release pattern, characterized by an initial "burst" release in the first 2 hours, where between 20% (MWCNTs-PEG1500-TMZ) and 41% (MWCNTs-G-PEG6000-TMZ) of TMZ was released, which is most likely related to the fraction of the drug located on or close to the surface of the nanocarriers. The sustained release phase lasted for the next eight days, during which almost the entire TMZ content was released (between 84% and 99% from MWCNTs-TMZ and MWCNTs-G-PEG6000-TMZ, respectively) (Fig. 2). Slower drug release from the PEGylated MWCNTs compared to non-PEGylated formulations during eight days was evident (Fig. 2a), probably due to the increased diffusion barrier formed from the PEG chains and concurrent behavior of TMZ and PEG on the carbon nanotubes surface, having in regard the hydrophilic nature of TMZ. Similar results were presented in the paper of Jain *et al.* [21], where slower TMZ release from PEGylated PLGA nanoparticles compared to non-PEGylated ones was observed. Furthermore, faster TMZ release from all hybrid

structures was noted compared to TMZ-loaded MWCNTs (Fig. 2b), probably due to the different ratios of the drug loaded inside the tubes and onto the surface of these different carbon nanostructures. The different PEGs did not cause different drug release patterns in MWCNTs and hybrid structures. From the dissolution curve of TMZ-loaded MWCNTs-G, it can be assumed that the graphene sheets probably block the drug's entrance into the tubes and subsequently restrict its location mainly on their surface, resulting in 99% of the drug being released within 10 hours.

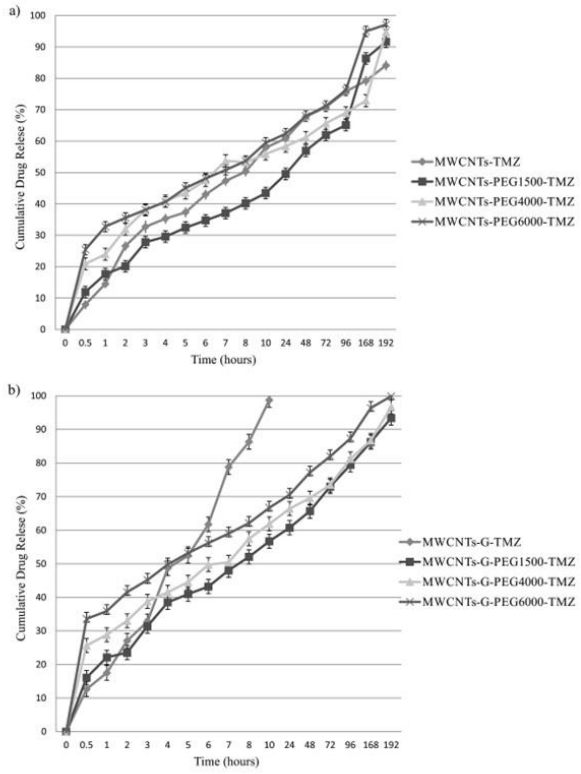

Figure 2. Cumulative TMZ release profile from (a) non-PEGylated and PEGylated MWCNTs and (b) non-PEGylated and PEGylated MWCNTs-G in medium with pH 7.4.

TMZ has a short half-life of 1.8 hours and requires repeated administration to maintain its efficacy. Hence, the controlled and sustained release of TMZ is a desired property for the developed nanoformulations because a prolonged drug release profile requires less frequent drug administration and reduces the toxic effects of TMZ [33]. Namely, it is well known that in terms of short- and long-term efficacy, the sustained-release chemotherapy within the tumor bed could significantly improve the therapeutic effect of patients with malignant recurrent glioma and prolong their survival [34]. Therefore, continuous chemotherapy with the slow-release of TMZ in tumor bed interstitium may promote postoperative radiotherapy sensitization, manifest a synergistic anti-tumor effect, kill tumor cells to a great extent, achieve a high clinical remission rate and improve the long-term survival of patients. In addition, preliminary *in vitro* and *in vivo* studies suggest that activated carbon nanostructures can be used as adjuvant therapy along with the standard treatment in malignant gliomas, concerning their capability to be endocytosed by tumor cells and induce lysosomal dysfunction and mitochondrial damage in the tumor cells [35].

Physicochemical characterization of Temozolomide loaded PEGylated carbon nanostructures

UV-Vis absorption spectroscopy

TMZ loading can be monitored using UV-Vis absorption spectroscopy because TMZ dissolved in water (0.1 mg/mL) displays two characteristic absorption peaks at 255 nm and 328 nm, corresponding to the active hydrolytic metabolite 5-(3-methyl triazen-1-yl) imidazole-4-carboxamide (MTIC) of TMZ and the prodrug TMZ, respectively. As shown in Fig. 3a and Fig. 3b, these two peaks did not appear in the free PEG, unloaded MWCNTs-(G)-COOH and MWCNTs-(G)-PEG. In the UV-Vis spectra of TMZ-loaded nanocarriers, MWCNTs-TMZ, MWCNTs-G-TMZ, MWCNTs-PEG-TMZ, MWCNTs-G-PEG-TMZ peaks at 328 nm and 255 nm clearly showed the successful loading of TMZ in the carbon nanocarriers.

Infrared spectroscopy

Infrared spectroscopy was performed to analyze the presence of different functional groups in the carbon nanocarriers and their interactions during PEG capping and TMZ loading (Fig. 4).

The oxidized carbon nanostructures MWCNTs-COOH and MWCNT-G-COOH (Fig. 4a and Fig. 4b, respectively) showed a characteristic band at 1695 cm^{-1} that can be ascribed to C=O stretching vibration of the carboxyl group. The observed shift of the C=O stretching band position to lower wavenumbers upon PEG modification (1665 cm^{-1}) is often attributed to the increased polarity and hydrogen bonding of the C=O functional group in the presence of PEG, leading to a more acidic C=O moiety. The shift can also result from a change in the local environment of the C=O functional group, such as changes in the molecular geometry and increased solvation. The shift should not be confused by the band at 1740 cm^{-1} that arises from the PEG, indicating the presence of the PEG moieties in the MWCNTs-PEG sample. In the PEGylated MWCNTs as well as in the non-PEGylated one, another band in the 3500–3400 cm^{-1} region can be observed, characteristic for H bonded O-H stretching vibrations from the PEG and the carboxylic OH group in the MWCNTs. In addition, three other bands emerged between 2950 cm^{-1} and 2850 cm^{-1}, typical for the C-H stretchings in both PEG and MWCNTs, being

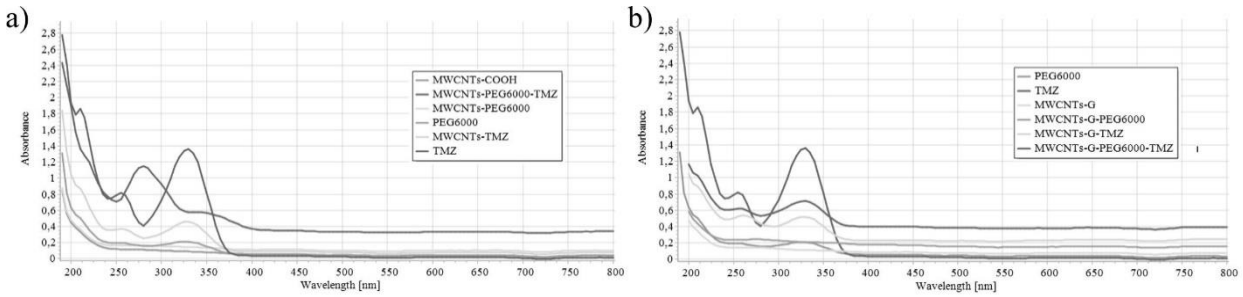

Figure 3. UV-Vis spectra of (a) TMZ, PEG, non-PEGylated and PEGylated blank, and TMZ loaded MWCNTs and (b) TMZ, PEG, non-PEGylated and PEGylated blank and TMZ loaded MWCNTs-G.

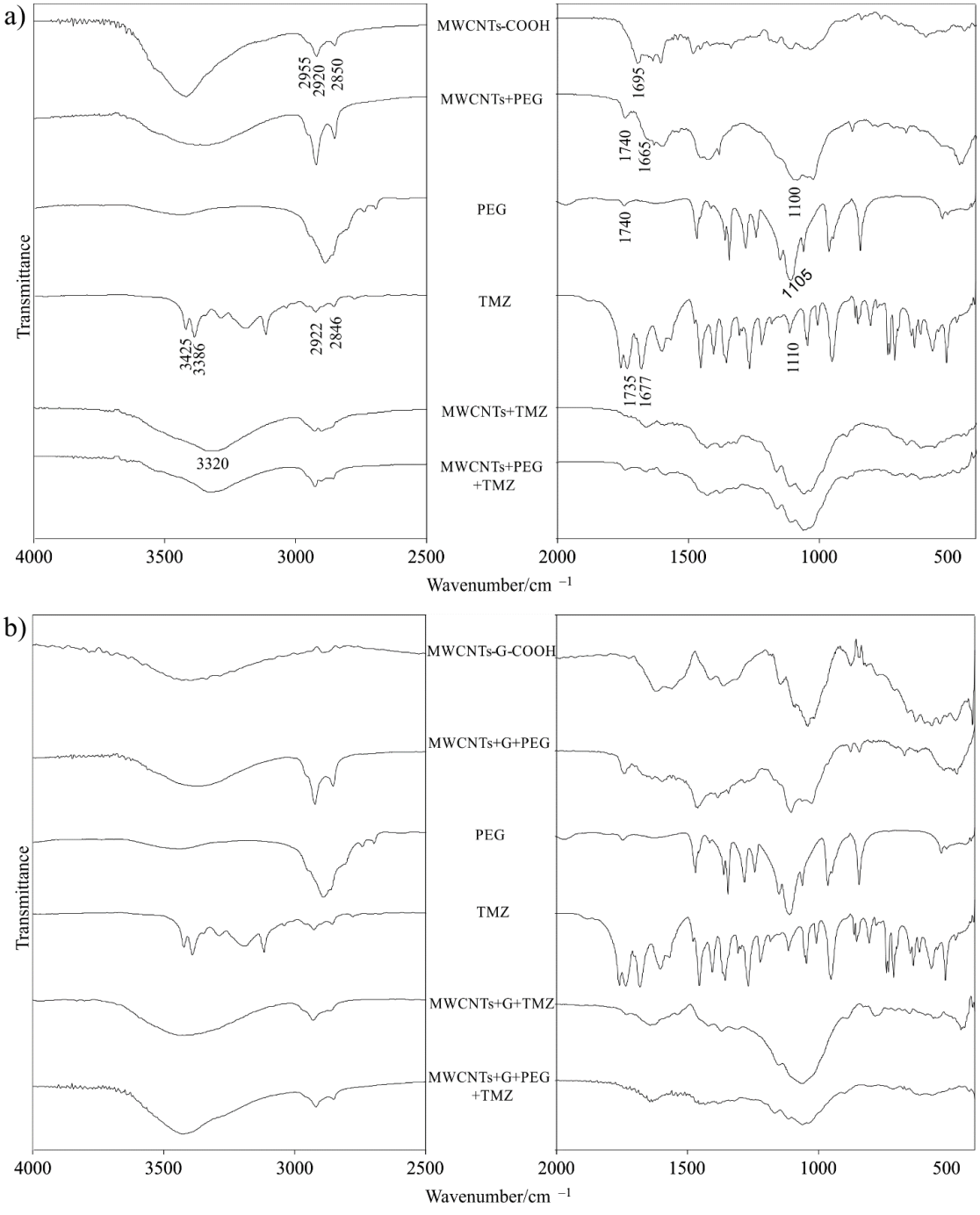

Figure 4. IR spectra of (a) TMZ, PEG, non-PEGylated and PEGylated blank, and TMZ loaded MWCNTs and (b) TMZ, PEG, non-PEGylated and PEGylated blank, and TMZ loaded MWCNTs-G.

more intense in the MWCNTs-PEG formulations. Moreover, a characteristic band at around 1100 cm^{-1} evolved in the spectra of MWCNTs-PEG, attributed to the C-O stretching vibration of the ether group in PEG. The band characteristic for PEG appeared both in the spectra of PEGylated formulations and pure PEG, again demonstrating the conjugation of PEG with MWCNTs.

To further examine the drug/carrier interactions, the IR spectra of blank and TMZ-loaded nanocarriers were analyzed (Fig. 4a, last three spectra). The IR spectrum of TMZ showed two broad bands at 3425 cm^{-1} and 3386 cm^{-1} attributed to the stretching vibration modes of N-H in NH_2, while the two bands at around 2922 cm^{-1} and 2846 cm^{-1} are related to the C-H stretch in position 6 and methyl group bonded to N in position 3. A band at around 1735 cm^{-1} in pure TMZ originates from the stretching C=O carbonyl vibration; the maximum at 1677 cm^{-1} corresponds to amide I mode, whereas the band at 1110 cm^{-1} is attributed to the C-N stretching vibration. TMZ loading in MWCNTs and MWCNTs-PEG weakened the hydrogen bonding, reducing the intensity and red-shifting the bands from 3420 cm^{-1} to 3320 cm^{-1}. Also, the other two C-H stretching bands positioned in the 2950-2850 cm^{-1} in spectra of the loaded particles appeared with obscured intensity. A similar behavior was observed for the strong band at around 1700 cm^{-1} in MWCNTs-COOH, which became weaker in the MWCNTs-TMZ spectrum (Fig. 4a), probably because the TMZ loading hindered to some extent the stretching carbonyl vibration by the interaction that affected the corresponding oxygen atoms. Furthermore, the peak at around 1100 cm^{-1}, characteristic of the C-N stretching band, was more intensive in the MWCNTs-TMZ compared to the MWCNTs-PEG-TMZ spectrum, which the difference in the TMZ loading can explain. The overall spectral impression is that the samples loaded by TMZ (MWCNTs-TMZ and MWCNTs-PEG-TMZ) do not markedly show characteristic TMZ bands either due to its low quantity or its likely position in the tunnels of the CNT, opposite to the larger PEG molecules that cannot easily enter and nest inside the tunneling regions.

In the spectrum of oxidized MWCNTs-G-COOH (Fig. 4b), the intensities of the bands mentioned above were not as strong compared to the spectrum of MWCNTs-COOH, which might suggest that the formulation with added graphene is less prone to oxidation and structural changes. However, in the spectrum of PEGylated MWCNTs-G, the characteristic bands at 3500–3400 cm^{-1}, 2950–2850 cm^{-1}, and 1100 cm^{-1} were also present, which indicates successful functionalization. TMZ loadings on the samples (MWCNTs-G-TMZ and MWCNTs-G-PEG-TMZ) led to a strong band at 3420 cm^{-1}, serving as a tracer for the presence of NH_2 group from TMZ. The intensity and shape of the infrared bands in the 2900–2800 cm^{-1} region were also changed, probably due to the interactions of these carbon nanocarriers with TMZ.

Overall, there was no strong similarity between the IR spectra of pure TMZ and that of the TMZ-loaded carbon nanostructures, suggesting the existence of electrostatic, hydrogen bonds, or/and Van der Waals forces between the TMZ molecules and the (PEGylated) carbon nanostructures. In addition, the functional groups in MWCNTs-(G)-COOH and MWCNTs-(G)-PEG could also overlap some of the TMZ bands in the IR spectrum, which were otherwise visible for the pure compound.

Raman spectroscopy

The functionalization of the carbon nanostructures can be further confirmed by Raman spectroscopy, which can provide molecular insights about the PEGylation and TMZ loading and the purity of the analyzed nanosystems. Two significant features evolve in the Raman spectrum of carbon nanostructures. The first spectral information is extracted from the D band, also known as the “disorder band,” typically located around 1350 cm^{-1}, related to the degree of the disordered (sp^3-hybridized) carbon atoms in the carbon nanostructures (MWCNTs or MWCNTs-G). The second is given by the position and intensity of the G band or tangential mode (1500–1600 cm^{-1}) consisting of two sub-bands, G^+ and G^-, related to axial and circumferential in-plane vibrations in semiconducting nanotubes. It is associated with the in-plane stretching of sp^2-hybridized carbon atoms in a hexagonal lattice. The broadening of the bands and the intensities of D and G bands can shed light on the extent of functionalization by determining the intensity ratio of both bands, I_D/I_G [36–38].

Fig. 5a and 5b nest the Raman spectra of pristine MWCNTs and MWCNTs-G and the functionalized MWCNTs-PEG and MWCNTs-G-PEG, respectively. It is evident that the intensity ratio I_D/I_G after the attachment of PEG onto the surface did not significantly alter the I_D/I_G ratio and agrees with other PEGylated systems [13,39]. However, the MWCNTs spectra upon TMZ loading showed broadening of the D band, which can be explained by introduction of functional groups on MWCNTs and MWCNTs-PEG surfaces (Fig. 5a). Furthermore, the loading resulted in the increase of its intensity in comparison to the G band, leading to $I_D/I_G > 1$ for MWCNTs-TMZ and MWCNTs-PEG-TMZ spectra, contrary to the pristine and PEGylated samples were $I_D/I_G < 1$. The trend of dominance of D over G band upon TMZ loading ($I_D/I_G > 1$) was also confirmed for the

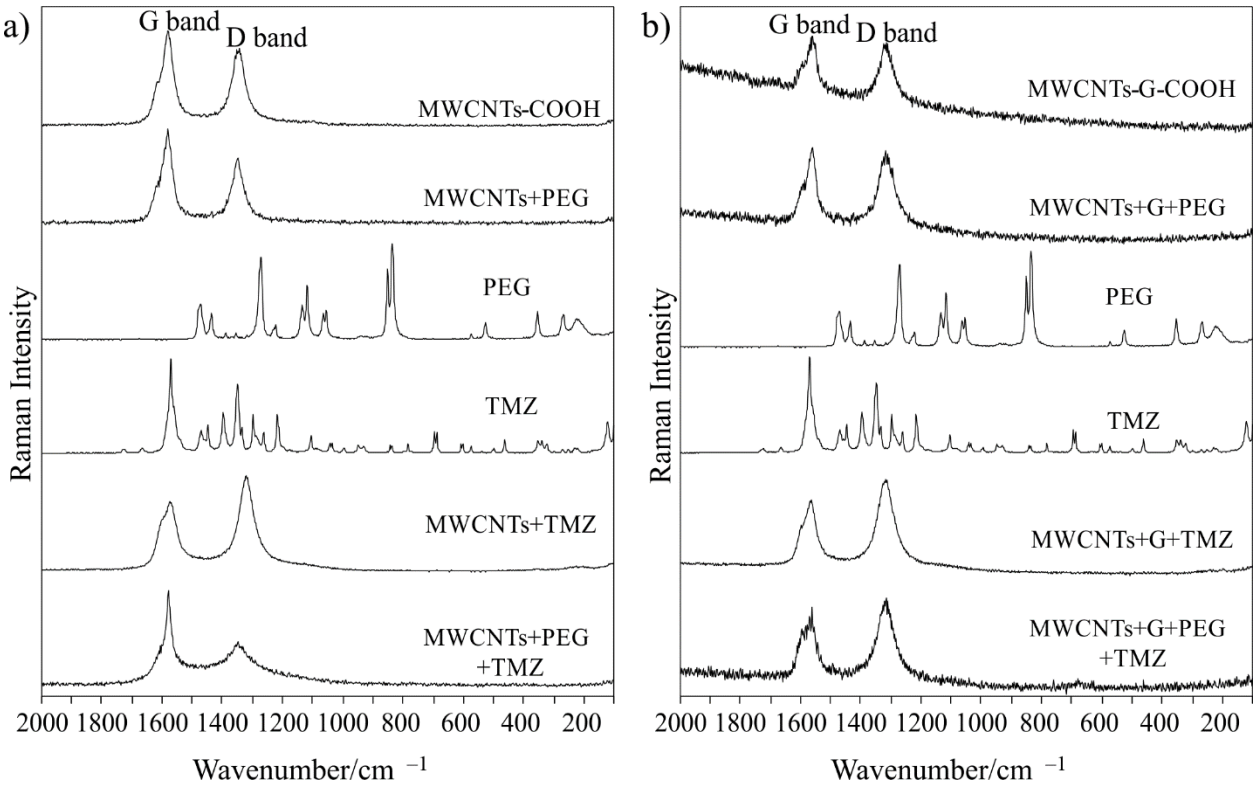

Figure 5. Raman spectra of (a) TMZ, PEG, non-PEGylated, and PEGylated blank and TMZ loaded MWCNTs and (b) TMZ, PEG, non-PEGylated and PEGylated blank, and TMZ loaded MWCNTs-G.

MWCNTs-G samples (Fig. 5b); the production of a higher number of defects in the functionalized material may explain this.

Thermogravimetric analysis

Thermogravimetric analysis was also used to explore and confirm the functionalization of MWCNTs-COOH and MWCNTs-G-COOH with PEG and the loading of TMZ. The results of TGA for both carrier groups are presented in Fig. 6a and 6b, respectively. The initial weight loss observed until 100 °C (in all formulations) was due to the water loss, as also pointed out by Zhao *et al.* [12]. In the weight loss profile of TMZ, there was a baseline temperature of 210 °C, shown also in the paper of Gürten *et al.* [40]. As shown in Fig. 6a, the weight of MWCNTs-COOH decreased with increasing temperature, but the weight loss was different compared to the weight loss of MWCNTs-PEG and PEG. Pure PEG weight decreased sharply with increasing temperature, showing almost 100% weight loss at ca. 400 °C. In the diagram of MWCNTs-PEG, 29% weight loss was noted at 800 °C, 10% more than that of MWCNTs-COOH. This weight loss was due to the decomposition of PEG chains. In the diagram of MWCNTs-TMZ, 22% loss at 800 °C was observed, which was only 3% more compared to the weight loss of pure MWCNTs-COOH, indicating strong interaction/entrapment of TMZ in MWCNTs-COOH. The weight loss of MWCNTs-PEG-TMZ at 800 °C was 19%, ca.10% less than that of MWCNTs-PEG, indicating that the drug/carrier interaction is much stronger in TMZ-loaded PEGylated systems.

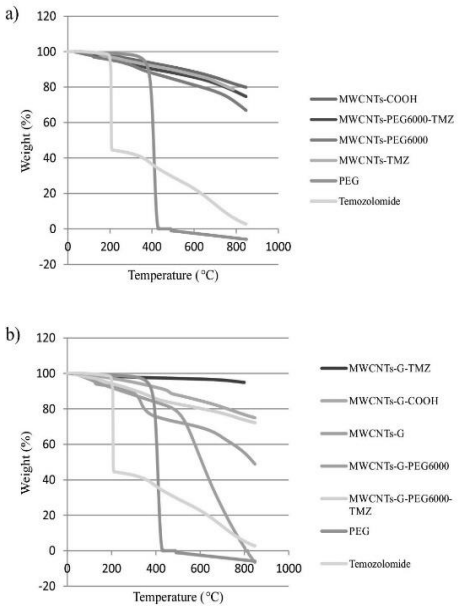

Figure 6. TGA plots of (a) TMZ, PEG, non-PEGylated and PEGylated blank, and TMZ loaded MWCNTs and (b) TMZ, PEG, non-PEGylated and PEGylated blank, and TMZ loaded MWCNTs-G.

In the TGA curve of MWCNTs-G (Fig. 6b), only one sharp weight loss peak before 500 °C was observed, indicating that the hybrid had a small amount of amorphous carbon and that the graphene and MWCNTs in the hybrid exhibit similar thermal stability. The same was observed by Zhao *et al.*, who fabricated and analyzed G/SWCNT hybrids [36]. The MWCNTs-G-COOH showed the highest thermal stability, with only 14% weight loss, which brought us to the fact that COOH groups crafted on the surface led to an increase in thermal stability. With modification and introduction of PEG molecules on the surface, a new thermo-diagram with two inclinations was formed. The first peak at approximately 115 °C resulted from the degradation of PEG, while the peak at 390 °C from the defects created during oxidation accordingly. When loaded with TMZ, the elevation of the decomposition temperature compared to the blank carriers indicates that strong interactions were formed between the drug and carriers (MWCNTs-G-COOH and MWCNTs-G-PEG).

CONCLUSION

In conclusion, the carbon nanostructures, MWCNTs, and their hybrid with graphene MWCNTs-G have been successfully functionalized with PEG and loaded with TMZ, an alkylating drug used to treat certain types of brain tumors. Simple procedures were used for functionalization and drug loading, providing relatively high TMZ loading and particle size and surface properties of the carbon nanocarriers suitable for crossing the BBTB and uptake into the tumor cells. As a desired property of the developed carbon nanocarriers, a sustained release of TMZ was achieved, suggesting the potential for less frequent TMZ administration and a better therapeutic index. Further studies are planned to evaluate the possible radiosensitization effect of TMZ-loaded carbon nanocarriers for glioma cells in vitro and in adequate animal models.

ACKNOWLEDGMENT

The authors express gratitude to the International Atomic Energy Agency (IAEA) for supporting this study, performed within the project for technical cooperation titled “Application of ionizing irradiation in nanotechnology (MAK1003)".

REFERENCES

[1] Y. Zhou, K. Vinothini, F. Dou, Y. Jing, A. A. Chuturgoon, T. Arumugam, M. Rajan, Arabian J. Chem. 15 (2022) 103649. https://doi.org/10.1016/j.arabjc.2021.103649.

[2] L. Wu, C. Man, H. Wang, X. Lu, Q. Ma, Y. Cai, W. Ma, Pharm. Res. 30 (2013) 412–423. https://doi.org/10.1007/S11095-012-0883-5

[3] R. Singh, N.K. Mehra, V. Jain, N.K. Jain, J. Drug Targeting 21 (2013) 581–592. https://doi.org/10.3109/1061186X.2013.778264.

[4] B. Zhang, Y. Xing, Z. Li, H. Zhou, Q. Mu, B. Yan, Nano Lett. 9 (2009) 2280–2284. https://doi.org/10.1021/nl900437n.

[5] D. Pantarotto, R. Singh, D. McCarthy, M. Erhardt, J.P. Briand, M. Prato, K. Kostarelos, A. Bianco, Angew. Chem. 43 (2004) 5242–5246. https://doi.org/10.1002/anie.200460437.

[6] A. Masotti, M.R. Miller, A. Celluzzi, L. Rose, F. Micciulla, P.W.F. Hadoke, S. Belluci, A. Caporali, Nanomed. Nanotehnol. Biol. Med. 12 (2016) 1511–1522. https://doi.org/10.1016/j.nano.2016.02.017.

[7] H. Sun, J. Ren, X. Qu, Acc. Chem. Res. 49 (2016) 461–470. https://doi.org/10.1021/acs.accounts.5b00515.

[8] N. Jawahar, A. De, S. Jubee, E.S. Reddy, Drug Dev. Res. 81 (2019) 305–314. https://doi.org/10.1002/ddr.21620.

[9] Y. Wu, J.A. Phillips, H. Liu, R. Yang, W. Tan, ACS Nano 2 (2008) 2023–2028. https://doi.org/10.1021/NN800325A.

[10] P. Wolski, K. Nieszporek, T. Panczyk, Phys. Chem. Chem. Phys. 19 (2017) 9300–9312. https://doi.org/10.1039/C7CP00702G.

[11] B.S. Wong, S.L. Yoong, A. Jagusiak, T. Panczyk, H.K. Ho, W.H. Ang, G. Pastorin, Adv. Drug Delivery Rev. 65 (2013) 1964–2015. https://doi.org/10.1016/j.addr.2013.08.005.

[12] X. Zhao, K. Tian, T. Zhou, X. Jia, J. Li, P. Liu, Colloids Surf. B 168 (2018) 43–49. https://doi.org/10.1016/j.colsurfb.2018.02.041.

[13] D. Ravelli, D. Merli, E. Quartarone, A. Profumo, P. Mustarelli, M. Fagnoni, RSC Adv. 3 (2013) 13569–13582. https://doi.org/10.1039/C3RA40852C.

[14] A. Di Martino, P. Kucharczyk, Z. Capakova, P. Humpolicek, V. Sedlarik, J. Nanopart. Res. 19 (2017) 1–16. https://doi.org/10.1007/s11051-017-3756-3.

[15] J.S. Ananta, R. Paulmurugan, T.F. Massoud, Neurol. Res. 38 (2016) 51–59. https://doi.org/10.1080/01616412.2015.1133025.

[16] A.A. John, A.P. Subramanian, M.V. Vellayappan, A. Balaji, H. Mohandas, S. Jaganathan, Int. J. Nanomed. 10 (2015) 4267–4277. https://doi.org/10.2147/IJN.S83777.

[17] C.Y. Lee, I.H. Ooi, Pharmaceuticals 9 (2016) 54. https://doi.org/10.3390/PH9030054.

[18] Q. Guo, X. Shen, Y. Li, S. Xu, Curr. Med. Sci. 37 (2017) 635–641. https://doi.org/10.1007/s11596-017-1783-z.

[19] H. Huang, Q. Yuan, J.S. Shah, R.D.K. Misra, Adv. Drug Delivery Rev. 63 (2011) 1332–1339. https://doi.org/10.1016/j.addr.2011.04.001.

[20] L. Niu, L. Meng, Q. Lu, Macromol. Biosci. 13 (2013) 735–744. https://doi.org/10.1002/mabi.201200475.

[21] A. Jain, G. Chasoo, S.K. Singh, A.K. Saxena, S.K. Jain, J. Microencapsulation 28 (2011) 21–28. https://doi.org/10.3109/02652048.2010.522257.

[22] X. Wei, X. Chen, M. Ying, W. Lu, Acta Pharm. Sin. B 4 (2014) 193–201.

https://doi.org/10.1016/j.apsb.2014.03.001.

[23] S. Honary, F. Zahir, Trop. J. Pharm. Res. 12 (2013) 255–264. https://doi.org/10.4314/tjpr.v12i2.19.

[24] Y. Yamamoto, Y. Nagasaki, Y. Kato, Y. Sugiyama, K. Kataoka, J. Controlled Release 77 (2001) 27–38. https://doi.org/10.1016/s0168-3659(01)00451-5.

[25] Y.Y. Yuan, C. Mao, X. Du, J. Du, F. Wang, J. Wang, Adv. Mater. 24 (2012) 5476–5480. https://doi.org/10.1002/adma.201202296.

[26] C. Saraiva, C. Praça, R. Ferreira, T. Santos, L. Ferreira, L. Bernardino, J. Controlled Release 235 (2016) 34–47. https://doi.org/10.1016/j.jconrel.2016.05.044.

[27] A. Prokop, J.M. Davidson, J. Pharma. Sci. 97 (2018) 3518–3590. https://doi.org/10.1002/jps.21270.

[28] H. Gao, Acta Pharm. Sin. B 6 (2016) 268–286. https://doi.org/10.1016/j.apsb.2016.05.013.

[29] N. Sciortino, S. Fedeli, P. Paoli, A. Brandi, P. Chiarugi, M. Severi, S. Cicchi, Int. J. Pharm. 521 (2017) 69–72. https://doi.org/10.1016/j.ijpharm.2017.02.023.

[30] X. Cui, B. Wan, Y. Yang, X. Ren, L. Guo, Sci. Rep. 7 (2017) 1–13. https://doi.org/10.1038/s41598-017-01746-9.

[31] J. Ren, S. Shen, D. Wang, Z. Xi, L. Guo, Z. Pang, Y. Qian, X. Sun, X. Jiang, Biomaterials 33 (2012) 3324–3333. https://doi.org/10.1016/j.biomaterials.2012.01.025.

[32] V. Miranda-Goncalves, R.M. Reis, F. Baltazar, Curr. Cancer Drug Targets 16 (2016) 388–399. https://doi.org/10.2174/1568009616666151222150543.

[33] A. Orza, O. Soriţău, C. Tomuleasa, L. Olenic, A. Florea, O. Pana, I. Bratu, E. Pall, S. Florian, D. Casciano, A. Biris, T. Yoshiyuki, Int. J. Nanomed. 8 (2013) 689–702. https://doi.org/10.2147/IJN.S37481

[34] L. Wang, Z. Wang, Z. Liang, G. Li, S. Duan, Y. Xi, Am. J. Transl. Res. 14 (2022) 5669–5676. https://www.ncbi.nlm.nih.gov/pmc/articles/PMC9452319/pdf/ajtr0014-5669.pdf.

[35] S. Romano-Feinholz, A. Salazar-Ramiro, E.M. Sandoval, R. Magaña-Maldonado, N.H. Pedro, E.R. López, G.A. Aguilar, A.S. Garcia, J. Sotelo, P.V. Cruz, B. Pineda, Int. J. Nanomedicine 12 (2017) 6005–6026. https://doi.org/10.2147/IJN.S139004.

[36] M.Q. Zhao, X.F. Liu, Q. Zhang, G.L. Tian, J.Q. Huang, W. Zhu, F. Wei, ACS Nano 6 (2012) 10759–10769. http://doi.org/10.1021/nn304037d.

[37] N. Hadidi, F. Kobarfard, N. Nafissi-Varcheh, R. Aboofazeli, Int. J. Nanomed. 6 (2011) 737–746. https://doi.org/10.2147/ijn.s17626.

[38] B.V. Farahani, G.R. Behbahani, N. Javadi, J. Braz. Chem. Soc. 27 (2016) 694–705. https://doi.org/10.5935/0103-5053.20150318.

[39] J. Chen, H. Liu, C. Zhao, G. Qin, G. Xi, T. Li, X. Wang, T. Chen, Biomaterials 35 (2014) 4986–4995. https://doi.org/10.1016/j.biomaterials.2014.02.032.

[40] B. Gürten, E. Yenigül, A.D. Sezer, S. Malta, Braz. J. Pharm. Sci. 54 (2018) e17513. http://dx.doi.org/10.1590/s2175-97902018000217513.

RADMILA MILENKOVSKA[1]
NIKOLA GESKOVSKI[1]
PETRE MAKRESKI[2]
ANITA GROZDANOV[3]
EMIL POPOVSKI[2]
GJORGJI PETRUSHEVSKI[2,4]
MAJA SIMONOSKA CRCAREVSKA[1]
KRISTINA MLADENOVSKA[1]

[1]Faculty of Pharmacy, Ss. Cyril and Methodius University in Skopje, Skopje, Republic of N Macedonia

[2]Institute of Chemistry, Faculty of Natural Sciences and Mathematics, Ss. Cyril and Methodius University in Skopje, Skopje, Republic of N Macedonia

[3]Faculty of Technology and Metallurgy, Ss. Cyril and Methodius University in Skopje, Skopje, Republic of N Macedonia

[4]Alkaloid AD Skopje, Skopje, Republic of N Macedonia

NAUČNI RAD

FUNKCIONALIZOVANE NANOSTRUKTURE UGLJENIKA KAO NOSAČI TEMOZOLOMIDA; FIZIČKOHEMIJSKA I BIOFARMACEUTSKA KARAKTERIZACIJA

U ovom radu, temozolomid (TMZ), lek koji se koristi u lečenju anaplastičnog astrocitoma i multiformnog glioblastoma, ugrađen je u višeslojne ugljenične nanocevi (VSUNC) i hibridne ugljenične nanocevi sa grafenom (VSUNC-G) funkcionalizovanim polietilen-glikolom (PEG). Cilj je bio da se proceni potencijal ovih nanonosača za ciljanu isporuku i produženo oslobađanje TMZ u ćelijama tumora mozga. Oksidovani VSUNC i VSUNC-G su nekovalentno funkcionalizovani sa PEG-ima različite molekulske mase i zatim je nanet TMZ prema standardnim procedurama. Temeljna fizičko-hemijska i biofarmaceutska karakterizacija nanonosača ugljenika sa nanetim TMZ ukazala je na visoku efikasnost inkapsulacije (do 67%) i punjenje lekom (do 18% od 25% teorijske vrednosti) i homogenu distribuciju veličine čestica, sa z-prosekom (160 do 300 nm) i zeta potencijala (-31mV do -21 mV) čestica adekvatnih za prelazak krvno-moždane-tumorske barijere i ulazak u tumorske ćelije. Uspešna funkcionalizacija i TMZ nanošenje potvrđeni su SEM i TEM slikama, UV-Vis apsorpcijom, infracrvenom i Raman spektroskopijom i TGA analizama. Produženo oslobađanje TMZ iz ugljeničnih nanonosača je zapaženo in vitro. Prikazani nalazi čine osnovnu platformu za dalje istraživanje ovih formulacija protiv različitih tipova ćelija glioma i na adekvatnim životinjskim modelima.

Ključne reči: višeslojne ugljenične nanocevi, grafen, polietilen-glikol, temozolomid, fizičko-hemijska svojstva, produženo oslobađanje.